

# Interfacial Stability of Layered $\text{LiNi}_x\text{Mn}_y\text{Co}_{1-x-y}\text{O}_2$ Cathodes with Sulfide Solid Electrolytes in All-Solid-State Rechargeable Lithium-Ion Batteries from First-Principles Calculations

Published as part of *The Journal of Physical Chemistry virtual special issue "Esther Sans Takeuchi Festschrift"*.

Hideyuki Komatsu, Swastika Banerjee, Manas Likhit Holekevi Chandrappa, Ji Qi, Balachandran Radhakrishnan, Shigemasa Kuwata, Kazuyuki Sakamoto, and Shyue Ping Ong\*



Cite This: <https://doi.org/10.1021/acs.jpcc.2c05336>



Read Online

ACCESS |



Metrics & More

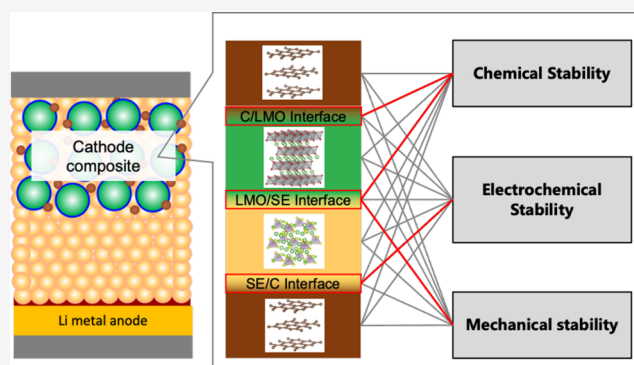


Article Recommendations



Supporting Information

**ABSTRACT:** Among the key impediments to the practical application of all-solid-state lithium-ion batteries are the reactions occurring at the interfaces between the electrode active material, the solid electrolyte, and conductive additives such as carbon. Here, we provide in-depth insights into the relationship between composition and interfacial stability with sulfide solid electrolytes for the layered  $\text{LiNi}_x\text{Mn}_y\text{Co}_{1-x-y}\text{O}_2$  (NMC) cathodes in widespread commercial applications today using density functional theory calculations. We show that increasing the Ni content and, to a lesser extent, increasing the Co content, has the effect of increasing reactivity with the  $\text{Li}_6\text{PS}_5\text{Cl}$  (LPSCI) solid electrolyte. This suggests that current efforts to reduce the Co content in cathodes may compromise potential application in all-solid-state architectures. However, we also find that common SEI phases such as  $\text{Li}_2\text{CO}_3$ , surface phases such as NiO, and oxide buffer layers such as  $\text{LiNbO}_3$  generally exhibit only limited reactivity with either  $\text{LiMO}_2$  or LPSCI. Hence, these phases, formed either in operando or added during synthesis, can potentially serve as effective barriers against further reaction, provided a uniform coating can be achieved.



## INTRODUCTION

All-solid-state batteries (ASSBs) are one of the most promising candidates for next-generation energy storage, owing to their advantages in balancing safety, high capacity, and higher power.<sup>1</sup> A schematic of an ASSB is given in Figure 1. Unlike conventional lithium-ion batteries utilizing liquid electrolytes, the use of a solid electrolyte (SE) makes the battery less flammable and, therefore, safer.<sup>2</sup> In addition, SEs can potentially enable the application of the Li metal anode, which is expected to lead to substantial increases in energy density.<sup>3</sup> The most well-established commercial cathodes are transition metal (TM) layered oxides with the general formula  $\text{LiMO}_2$  (LMO), where M is either a single transition metal (e.g., Co or LCO) or a mixture of transitional metals (e.g.,  $\text{Ni}_x\text{Mn}_y\text{Co}_{1-x-y}$  or NMC). In recent years, there has been a push toward reducing the use of expensive Co metal in cathodes, i.e., the so-called Ni-rich NMCs.<sup>4–7</sup>

While there has been great progress in the development of SEs with extremely high ionic conductivities,<sup>8–12</sup> the chemical, electrochemical, and mechanical stabilities of the heterogeneous solid–solid interfaces in ASSBs remain key impediments to their widespread application. In particular, sulfide SEs,

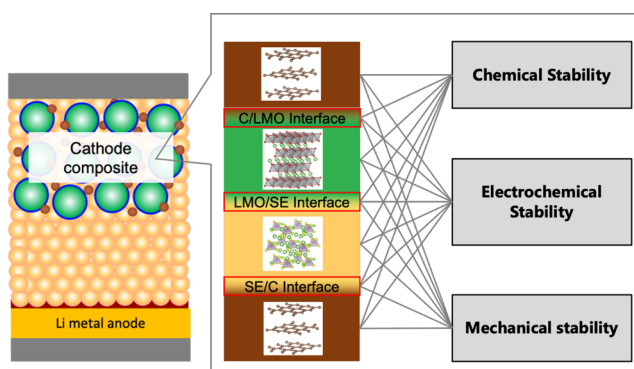


**Figure 1.** Schematic diagram of an all-solid-state lithium-ion battery and the interfaces present between the cathode active material, solid electrolyte, and carbon additives.

Received: July 28, 2022

Revised: September 28, 2022

which have exhibited the highest ionic conductivities in general, have relatively poor intrinsic chemical and electrochemical stabilities, especially against commercial oxide cathodes.<sup>13–25</sup> For instance, chemical reactivity and mutual diffusion have been demonstrated both experimentally and theoretically at the LCO and the sulfide SE ( $\text{Li}_2\text{S}-\text{P}_2\text{S}_5$ <sup>26</sup> and  $\text{Li}_3\text{PS}_4$ <sup>24</sup>) interface. Cells based on uncoated LCO and sulfide SEs exhibit increasing interfacial resistance upon cycling and poor cell characteristics compared to traditional liquid electrolyte cells.<sup>27</sup> Other common cathodes such as  $\text{LiMn}_2\text{O}_4$ , NMC, and NCA have also been reported to exhibit similar interfacial instability with sulfide SEs.<sup>14,20</sup> Interfacial reactivity can be mitigated to some extent by coating the cathode with oxides such as  $\text{LiNbO}_3$ ,<sup>27</sup> though with potentially additional cost and decreased cell performance.<sup>20</sup>

Several gaps remain in our understanding of cathode/SE interfacial reactivity. First, most computational studies<sup>13</sup> have focused on the single-TM layered oxides, and less emphasis has been placed on the mixed-TM NMC cathodes that increasingly dominate commercial applications. In particular, there is a lack of understanding as to the effect of the broader trend toward lowering Co/increasing Ni content on the interfacial reactivity in ASSBs. Second, besides the active material, other phases such as additive carbon and Li-containing impurities (e.g.,  $\text{Li}_2\text{CO}_3$ ) are present in the cathode, and their effect on interfacial reactivity is typically ignored in computational studies. Most of the research on the effect of carbon on interfacial reactivity is on the carbon/SE interface.<sup>21,28–30</sup>

In this work, we provide an analysis of interfacial reactivity between the NMC cathode active material, carbon additive, and the highly promising  $\text{Li}_6\text{PS}_5\text{Cl}$  argyrodite (LPSCI) SE in ASSBs based on density functional theory (DFT) calculations. A crucial finding is that an increased Ni content leads to increased interfacial reactivity, indicating that there is a tension between current trends to reduce the use of expensive Co and the effort to realize safer ASSB architectures.

## METHODS

**Materials Selection and Data.** Where available, the precomputed structures and energies were obtained from the Materials Project.<sup>31–33</sup> Any DFT calculations were performed using the Vienna *Ab initio* Simulation Package (VASP)<sup>34</sup> within the projector-augmented wave approach<sup>35</sup> using the Perdew-Bruke-Ernzerhof (PBE) generalized gradient approximation (GGA) functional.<sup>36</sup> The key parameters were chosen to be compatible with the existing calculations in the Materials Project database, such as a plane wave energy cutoff of 520 eV, a *k*-point density of at least 1000/(number of atom), and Hubbard *U* parameters of 6.20, 3.32, and 3.90 eV for Ni, Co, and Mn, respectively, for oxides.

Figure 1 provides an overview of the interfaces between the cathode active material, SE, and conductive additives investigated. The specific materials investigated in this work, together with their corresponding Materials Project identifier, are as follows:

1. Cathode active material: Our goal is to investigate the effect of composition within the layered  $\text{LiNi}_y\text{Mn}_z\text{Co}_{1-y-z}\text{O}_2$  (NMC) O3 oxides (space group:  $R\bar{3}m$ ) on interfacial stability. As such, we have selected  $\text{LiCoO}_2$  (LCO, mp-22526),  $\text{LiNiO}_2$  (LNO, mp-25411),  $\text{LiNi}_{0.5}\text{Mn}_{0.5}\text{O}_2$  (NM11, mp-754945),  $\text{Li}$

$\text{Ni}_{1/3}\text{Mn}_{1/3}\text{Co}_{1/3}\text{O}_2$  (NMC111, mp-1222510), and  $\text{LiNi}_{5/6}\text{Mn}_{1/12}\text{Co}_{1/12}\text{O}_2$  (“high-Ni”, mp-1120802) for investigation. It should be noted that the chosen “high-Ni” composition corresponds to a Ni:Mn:Co ratio of 10:1:1, which approximates the commercial NMC811 composition within a reasonable  $2 \times 2 \times 1$  supercell of the conventional layered unit cell (48 atoms). We also considered  $\text{LiNi}_{0.8}\text{Co}_{0.15}\text{Al}_{0.05}\text{O}_2$  (NCA) as a commercial cathode active material. The NCA structure was generated by substituting Co to Al based on the lowest energy configuration of  $\text{LiNi}_{0.8}\text{Co}_{0.2}\text{O}_2$ . Collectively, these cathode materials shall henceforth be referred to as LMO for brevity.

2. Solid electrolyte: The  $\text{Li}_6\text{PS}_5\text{Cl}$  argyrodite (LPSCI, mp-985592) was selected as the SE because of its high ionic conductivity ( $\sigma = 1.33 \times 10^{-3} \text{ S cm}^{-1}$  at 25 °C)<sup>37</sup> and good cell performance.<sup>38</sup> In addition, the passivation phase generated at the interface between the cathode coating layer and LPSCI during the initial charge is highly stable.<sup>20</sup>
3. Additive: We have selected the most stable graphite structure from MP (C, mp-569304) as a conductive additive carbon.

## Chemical, Electrochemical, and Mechanical Stability.

The chemical, electrochemical, and mechanical stability of the interfaces were evaluated using several metrics that have already been well-established in prior works.<sup>39–44</sup> Here, we will provide a brief summary and clarify the definitions as they are used in this work. Interested readers are also referred to those prior works for further details.

A schematic of a pseudobinary phase diagram between A and B, for instance, between an electrode and a solid electrolyte, is shown in Figure 2. Following Zhu et al.,<sup>39</sup> we define the mutual reaction energy  $\Delta E_{D, \text{mutual}}(A, B)$  of the interface between two materials A and B (e.g., a cathode active material and a solid electrolyte) as the difference between the convex hull energies as the materials A and B at a particular ratio *x* and the corresponding linear combination of the hull

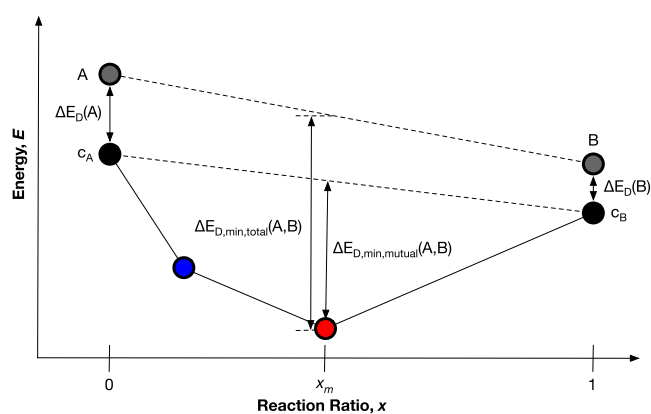


**Figure 2.** Schematic of a pseudobinary phase diagram between two materials A and B, which are assumed to be above the convex hull (black circles). The distance of A/B from the convex hull is the decomposition energy of A/B ( $\Delta E_{D, \text{total}}(A/B)$ ). The minimum of the mutual reaction energy  $\Delta E_{D, \text{min, mutual}}(A, B)$  is indicated in the figure, and the composition  $x_m$  at which this occurs is indicated by the red circle. The corresponding total reaction energy is ( $\Delta E_{D, \text{min, total}}(A, B)$ ) and includes the decomposition energies of A and B.

energies at the compositions of A and B ( $c_A$  and  $c_B$ ). The minimum of the mutual reaction energy  $\Delta E_{D, \min, \text{mutual}}(A, B)$  is given by

$$\Delta E_{D, \min, \text{mutual}}(A, B) = \min_{x \in [0, 1]} \frac{1}{N} \{E_{\text{eq}}[xc_A + (1-x)c_B] - xE[c_A] - (1-x)E[c_B]\} \quad (1)$$

where  $x$  is the ratio of A,  $E[c_A]$  and  $E[c_B]$  are the DFT total energies at the convex hull at the composition of phases A and B, respectively, and  $N$  is a normalization factor, which is equal to the total number of atoms involved in the reaction.  $E_{\text{eq}}(c)$  is the energy of phase equilibria at composition  $c$ . It should be noted that the mutual reaction energy does not include the decomposition energies of phases A and B. We may also define a corresponding total reaction energy  $\Delta E_{D, \min, \text{total}}(A, B)$ , which includes the linear combination of the decomposition energies of A and B ( $\Delta E_D(A)$  and  $\Delta E_D(B)$ , respectively). By definition,  $|\Delta E_{D, \min, \text{mutual}}(A, B)| \geq |\Delta E_{D, \min, \text{total}}(A, B)|$ . Both  $\Delta E_{D, \min, \text{mutual}}(A, B)$  and  $\Delta E_{D, \min, \text{total}}(A, B)$  can be considered estimates of the *chemical stability* of the interface. The more negative the  $\Delta E_{D, \min, \text{mutual}}(A, B)$  or  $\Delta E_{D, \min, \text{total}}(A, B)$ , the greater the thermodynamic driving force for the reaction between A and B. The difference between  $\Delta E_{D, \min, \text{mutual}}(A, B)$  and  $\Delta E_{D, \min, \text{total}}(A, B)$  is the contribution of the metastability of the end members to the interfacial instability. All DFT total energies were adjusted using the mixing scheme implemented within the Materials Project for phase stability analysis using a mix of GGA calculations with or without Hubbard (+U).<sup>45</sup>

Interfaces in rechargeable lithium-ion batteries, however, are open with respect to (wrt) lithium. The relevant thermodynamic potential under such conditions is the grand potential wrt Li, given by  $\Phi = E - \mu_{\text{Li}}N_{\text{Li}}$  where  $\mu_{\text{Li}}$  is the chemical potential of Li, and  $N_{\text{Li}}$  is the number of Li. The chemical potential of Li can be related to the applied voltage  $\phi$  in a rechargeable battery as  $\phi = \frac{\mu_{\text{Li}} - \mu_{\text{Li}}^0}{e}$ , where  $\mu_{\text{Li}}^0$  is the chemical potential of bulk Li, and  $e$  is the electron charge. Similarly, we can define a mutual and total reaction grand potential  $\Delta\Phi_{D, \min, \text{mutual}}(A, B)$  and  $\Delta\Phi_{D, \min, \text{total}}(A, B)$  for the reaction between A and B, which can be obtained by constructing the pseudobinary phase diagram between A and B using the calculated grand potentials for a given  $\mu_{\text{Li}}$  (or equivalently, applied potential).  $\Delta\Phi_{D, \min, \text{mutual}}(A, B)$  and  $\Delta\Phi_{D, \min, \text{total}}(A, B)$  can therefore be interpreted as a measure of the *electrochemical stability* of the interface. It should be noted that for grand potential analysis, the normalization factor  $N$  is given by the total number of atoms excluding Li.

Finally, volume changes during the operation of a battery can result in fracture and/or a loss of contact at the interface, therefore, adversely affecting electrochemical performance. We can estimate the percentage volume change  $\Delta V$  as a result of the reaction at a heterogeneous interface by comparing the volumes of products of the reaction to that of the reactants in the reaction. The final DFT relaxed volumes of each reactant/product are used in this estimate. A negative  $\Delta V$  means that the volume of the products is smaller than that of the reactants, leading to the formation of voids. On the other hand, a positive  $\Delta V$  means that the volume of the products is larger than that of the reactants, which may cause the buildup of stresses and cracks at the interface.

Finally, volume changes during the operation of a battery can result in fracture and/or a loss of contact at the interface, therefore, adversely affecting electrochemical performance. We can estimate the percentage volume change  $\Delta V$  as a result of the reaction at a heterogeneous interface by comparing the volumes of products of the reaction to that of the reactants in the reaction. The final DFT relaxed volumes of each reactant/product are used in this estimate. A negative  $\Delta V$  means that the volume of the products is smaller than that of the reactants, leading to the formation of voids. On the other hand, a positive  $\Delta V$  means that the volume of the products is larger than that of the reactants, which may cause the buildup of stresses and cracks at the interface.

## RESULTS AND DISCUSSION

**LMO/LPSCI Interfaces.** Figure 3 shows the calculated chemical reaction energies between various LMO/LPSCI

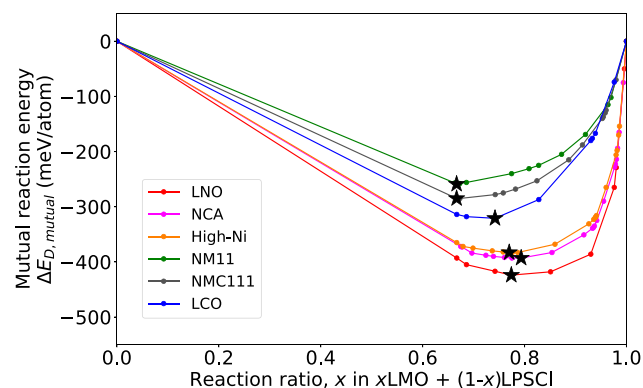


**Figure 3.** Pseudobinary phase diagram of LMO/LPSCI. The star marker indicates the most negative reaction energy and the thermodynamically favored reaction.

interfaces and the corresponding reaction products are listed in Table S1. Among the single-TM layered oxides, LNO is predicted to have a higher reactivity with the LPSCI SE than LCO. The reaction energy between LCO and LPSCI is about  $-320$  meV/atom, which is consistent with previously reported reaction energies between LCO and other sulfide SEs (LPS and LGPS).<sup>39</sup> One common reaction product is  $\text{Li}_3\text{PO}_4$ , which arises from S for O exchange reactions in the LPSCI solid electrolyte.<sup>24</sup> Interestingly, the Ni-containing NMC111 and NM11 are predicted to have substantially lower reactivity (higher reaction energies) than LNO and LCO. One potential explanation for this observation is the existence of Mn. Mn is in the 4+ oxidation state in the layered cathode, and even upon reaction with the SE, it either retains a formal 4+ oxidation state (e.g.,  $\text{MnS}_2$ )<sup>46</sup> or is only slightly reduced to a 3.5+ oxidation state (e.g.,  $\text{LiMn}_2\text{S}_4$  spinel)<sup>47</sup>. When Mn is present,  $\text{Li}_3\text{PO}_4$  is the only reaction product containing the oxygen anion, and the  $\text{S}^{2-}$  anion does not oxidize. In the absence of Mn, however, the Ni and Co undergo substantial reduction, with the concomitant oxidation of the  $\text{S}^{2-}$  anion to form  $\text{Li}_2\text{SO}_4$ . The formation of metal sulfides and  $\text{Li}_2\text{SO}_4$  with large valence changes is likely the main factor of the more exothermic reaction energy. However, further increase in the Ni content in the NMC system, i.e., the high-Ni composition, results in a substantial increase in reactivity with LPSCI.

Figure 4 shows the calculated ternary contour diagram of the reactivity of LMO/LPSCI interfaces within the Ni–Mn–Co system. The ternary contour diagram of the reactivity of the  $\text{LiNi}_x\text{Mn}_y\text{Co}_{1-x-y}\text{O}_2/\text{LPSCI}$  interface was constructed using 32 existing  $\text{LiNi}_x\text{Mn}_y\text{Co}_{1-x-y}\text{O}_2$  layered materials in the Materials Project database (see Table S2), including the three end members (LNO, LCO, and LMO), 24 binaries ( $\text{LiNi}_x\text{Mn}_{1-x}\text{O}_2$ ,  $\text{LiMn}_x\text{Co}_{1-x}\text{O}_2$ , and  $\text{LiCo}_x\text{Ni}_{1-x}\text{O}_2$ ), and 4 ternary compositions. The heat map was obtained by linearly interpolating between these data points. The stability order of the interface with LPSCI is  $\text{Mn} > \text{Co} > \text{Ni}$ . Even for  $\text{LiMnO}_2$ , the reaction energy is exothermic at around  $\sim -200$  eV/atom. This qualitative trend is in general agreement with previous reports. Auvergniot et al.<sup>14</sup> previously studied the reactivity of LCO, NMC111, and  $\text{LiMn}_2\text{O}_4$  with LPSCI using XPS. It was found that LCO and NMC111 exhibited similar levels of

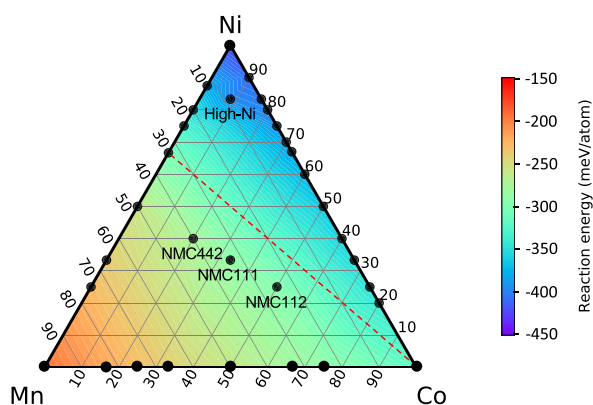


**Figure 4.** Ternary contour diagram of the reaction energy at the LMO/LPSCl interfaces. The 32  $\text{LiNi}_y\text{Mn}_z\text{Co}_{1-y-z}\text{O}_2$  layered compositions that were already present in the Materials Project are labeled with round markers and tabulated in Table S2. The heat map is obtained via interpolation from the computed reaction energies of the marked compositions. The red dashed line connecting LCO and  $\text{LiNi}_{0.7}\text{Mn}_{0.3}\text{O}_2$  indicates the trend line of the Co less cathode active material maintaining the same chemical stability.

chemical reactivity with LPSCl, in line with our results. From Figure 4, it may be readily observed that increasing the Ni content leads to increased reactivity with the LPSCl solid electrolyte, suggesting an inherent trade-off between the Ni content and interfacial stability in NMC-based all-solid-state battery systems.

Figure 5a shows the mutual and total reaction grand potential  $\Delta\Phi_{D, \min, \text{mutual}}$  and  $\Delta\Phi_{D, \min, \text{total}}$  respectively, of LMO/LPSCl interfaces as a function of applied potential. While the  $\Delta\Phi_{D, \min, \text{mutual}}$  and  $\Delta\Phi_{D, \min, \text{total}}$  remain relatively similar up to an applied potential of around 3 V, the differences widen significantly at the high voltage region. Above 4.5 V, the type of cathode active material has little effect on  $\Delta\Phi_{D, \min, \text{total}}$  indicating that much of the interfacial instability arises from the narrow electrochemical window of the solid electrolyte LPSCl itself (see Figure S3).<sup>13,44</sup> This observation is consistent with the results on the LCO/LPS and LCO/LGPS interfaces by Zhu et al.<sup>39</sup> The plot of the reaction molar ratio against the applied potential (Figure 5b) clearly shows that the LPSCl accounts for a large proportion of the reaction molar ratio at high voltage, while the cathode active material accounts for the majority of the reaction molar ratio at the low voltage region. However, the higher the Ni ratio, the more the active material tends to contribute to the decomposition reaction even at higher potentials.

**LMO/Carbon and LPSCl/Carbon Interfaces.** Carbon is a common additive used to increase the electronic conductivity in the electrodes.<sup>48</sup> Figure 6a and 6b show the reaction energies between various LMO/C and LPSCl/C interfaces, respectively. Somewhat surprisingly, we find that the LMO/C interface is chemically unstable. The trends in chemical stability of the LMO/C interface are similar to those for the LMO/LPSCl interfaces. The reaction products are dominated by the formation of  $\text{Li}_2\text{CO}_3$  and transition metal carbonates as shown in Table S1. These results are consistent with recent experimental reports of the formation of  $\text{Li}_2\text{CO}_3$  with carbon coating on the high-Ni cathode.<sup>49</sup> The formation of carbonates, which are well-known solid electrolyte interphase (SEI) components in traditional liquid electrolyte LIBs, may

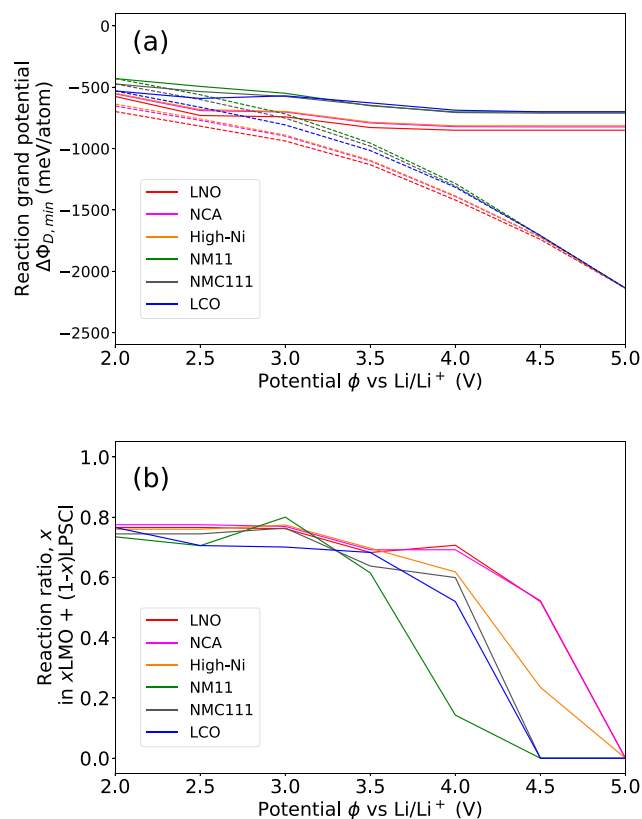


**Figure 5.** (a) The mutual reaction grand potential  $\Delta\Phi_{D, \min, \text{mutual}}$  (solid lines) and the total reaction grand potential  $\Delta\Phi_{D, \min, \text{total}}$  (dashed lines) under applied potential  $\phi$  in a 2–5 V range. (b) The relationship between the applied potential and the reaction ratio  $x_m$  of the most exothermic decomposition reaction.

serve as a passivation layer that prevents further reaction.<sup>50–53</sup> Phase transformations occurring at the electrode surface, such as the transformation of the layered cathode to rock-salt structure such as NiO,<sup>54</sup> may also protect the electrode against further reaction with C. Figure 6c and 6d show the calculated chemical and electrochemical reaction energies at 4.5 V between LMO/LPSCl/C and various surface/interphase/coating phases, respectively. In general, the LMO cathodes as well as C additive are predicted to be relatively chemically stable against NiO surface phases and  $\text{LiNbO}_3$  coating as well as the  $\text{Li}_2\text{CO}_3$  interphase. However, under an applied potential, the reactivity of the C additive substantially increases.

While the LPSCl SE is still predicted to be chemically and electrochemically unstable against the oxide surface/interface phases, the magnitudes of the reaction energies against the  $\text{LiNbO}_3$  buffer layer and  $\text{Li}_2\text{CO}_3$  interphase are much smaller in magnitude compared to that against the active LMO cathode or the NiO surface phase. Furthermore, any reaction between LPSCl and these oxides results in the formation of highly stable  $\text{Li}_3\text{PO}_4$  via a  $\text{S}^{2-}$  for  $\text{O}^{2-}$  exchange reaction, consistent with previous studies.<sup>23,43,55</sup> This  $\text{Li}_3\text{PO}_4$  may also serve as a potential passivating layer against further reactions.

The LPSCl/C interface is predicted to be chemically stable, which is consistent with XPS measurements on the pristine LPSCl-C electrode composite previously reported by Tan et al.<sup>29</sup> The XPS results for the S 2p and P 2p regions show no signals from other components in the pristine electrode for the

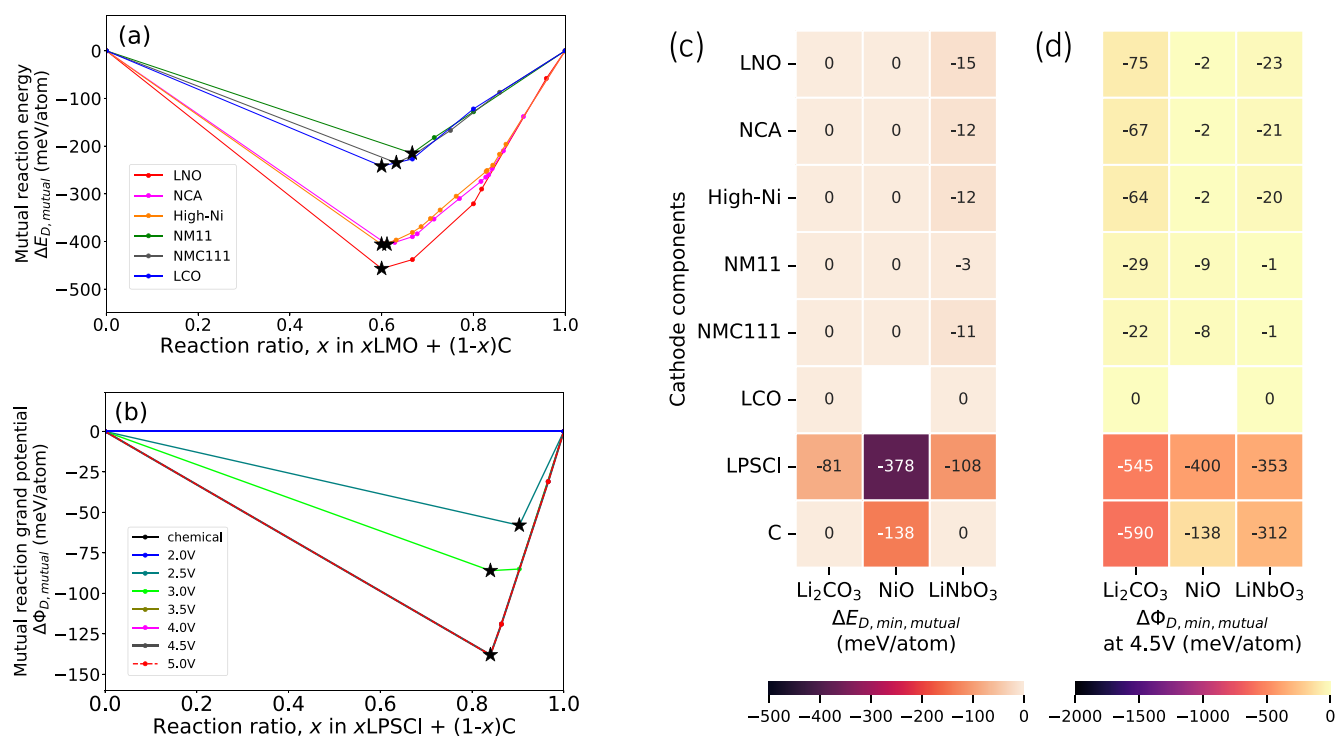


**Figure 6.** (a) Pseudobinary phase diagram of the LMO/C interface. (b) Pseudobinary mutual reaction grand potential  $\Delta \Phi_{D,mutual}$  phase diagram under different applied potentials of the LPSCl/C interface. The star marker indicates the most thermodynamically favored reaction under each condition. (c) Chemical reaction energies and (d) electrochemical reaction energies at 4.5 V between LMO/LPSCl/C and surface/interphase/coating phases.  $\text{LiNbO}_3$  is used as a representative oxide cathode coating material studied extensively in the literature.

electrode, which was well mixed by ball milling for 2 h at room temperature and at 300 rpm.

**Volume Change after Interfacial Reaction.** Volume changes at the electrode/solid electrolyte interphase can lead to contact loss and/or cracking, severely degrading cycling performance. Based on the predicted decomposition reactions in the preceding sections, we have estimated the percentage volume changes due to the interfacial reactivity, as shown in Figure 7. In all cases, LMO/LPSCl interfacial chemical reactions result in volume shrinkages exceeding 10%. The main reason for the shrinkage is the formation of  $\text{Li}_3\text{PO}_4$ ,  $\text{Li}_2\text{SO}_4$ ,  $\text{LiCl}$ , and metal sulfide, which have much higher densities (Tables S4 to S9). At a voltage of 4.5 V, the volume shrinkage is even larger at >30% due to the extraction of Li from the interface. We therefore expect interfacial reactions to result in contact loss between the active material and the SE. It should be noted that it is well-known that the volume of Ni-based cathode active materials shrinks upon delithiation, which would further exacerbate the contact loss at high voltages.<sup>56</sup> In contrast, the LMO/C interfacial chemical reactions result in a small volume expansion of 10% or less, which may somewhat mitigate the volume contraction due to LMO/LPSCl reactions. Here, the formation of  $\text{Li}_2\text{CO}_3$ , which accounts for 60% or more of the reaction product by volume ratio, is responsible for the volume expansion (Tables S4 to S9). However, the LMO/C interfacial electrochemical reactions at high voltages also result in substantial volume contraction of 17–23%, which is again associated with the extraction of Li from the system.

## CONCLUSIONS

To conclude, we have carried out a comprehensive study of layered LMO cathode/LPSCl interfaces using DFT calcu-

lations. The key finding is that there is an inherent trade-off between the overall drive toward reducing the Co content in layered LMO cathodes in recent years and the interfacial stability with solid electrolytes such as LPSCl. The higher Ni content leads to higher interfacial reactivity with LPSCl. The ternary contour plot as shown in Figure 4 provides a highly useful design tool. For instance, the plot suggests that one potential strategy to reduce the Co content while maintaining the same chemical stability as LCO is to move along the tie-line connecting LCO and  $\text{LiNi}_{0.7}\text{Mn}_{0.3}\text{O}_2$ , which has been reported as a Co-free cathode with high reversible capacity and cyclability.<sup>57</sup> We also find that the LMO/LPSCl interfaces become much more reactive at high voltages. Another major issue associated with cathode/SE interfaces is the volume change as a result of interfacial reactions. Large volume reductions of between 10% and 34% are predicted for LMO/LPSCl interfacial reactions, which would lead to potential contact loss between the cathode and the SE.

In addition, we also investigated the effect of the common carbon additive as well as other potential surface/interphase phases on the chemical reactivity at the interface. While C itself is predicted to be highly reactive with both LMO and LPSCl, one of the main products of the reaction with LMO is  $\text{Li}_2\text{CO}_3$ , a common SEI phase found in traditional liquid-electrolyte LIBs. A key result is that the  $\text{Li}_2\text{CO}_3$  SEI phase, surface phases such as NiO, and oxide buffer layers such as  $\text{LiNbO}_3$  generally exhibit only limited reactivity with either LMO or LPSCl. Hence, these phases, formed either in operando or added during synthesis, can potentially serve as effective barriers against further reaction, provided a uniform coating can be achieved.

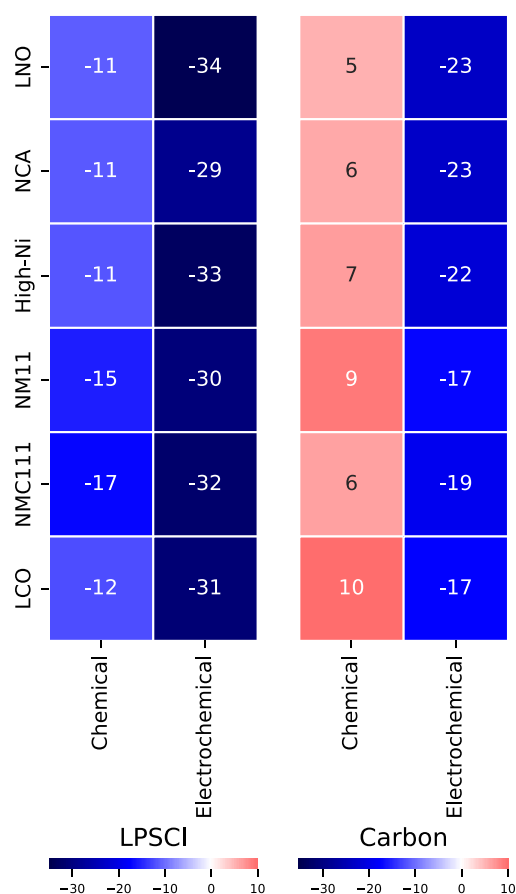


**Figure 7.** Percentage volume changes due to the chemical reaction and electrochemical reaction at 4.5 V at LMO/LPSCI (left) and LMO/C interfaces (right).

## ASSOCIATED CONTENT

### Supporting Information

The Supporting Information is available free of charge at <https://pubs.acs.org/doi/10.1021/acs.jpcc.2c05336>.

Mutual reaction grand potential  $\Delta\Phi_{D,mutual}$  and total reaction grand potential  $\Delta\Phi_{D,total}$  phase diagram under different applied potentials of LCO/LPSCI and  $\text{Li}_2\text{CO}_3$ /LPSCI interfaces; equilibrium voltage profiles of LPSCI with corresponding phase equilibria; total reaction grand potential  $\Delta\Phi_{D,total}$  phase diagram under different applied potentials of LPSCI/C interface; mutual reaction grand potential  $\Delta\Phi_{D,mutual}$  phase diagram under different applied potentials of  $\text{Li}_2\text{CO}_3$ /C interface; total reaction grand potential  $\Delta\Phi_{D,total}$  phase diagram under different applied potentials of  $\text{Li}_2\text{CO}_3$ /C interface; most probable reaction products and reaction energy of LMO/LPSCI and LMO/C interfaces; sources of crystal structures and reaction energies of ternary diagram of LMO/LPSCI interfaces; reaction formula and valence state of the composition in LMO/LPSCI interfaces; and sources of volume change of LMO/LPSCI and LMO/C interfaces (PDF)

## AUTHOR INFORMATION

### Corresponding Author

Shyue Ping Ong – Department of NanoEngineering, University of California, San Diego, La Jolla, California 92093-0448, United States; [orcid.org/0000-0001-5726-2587](https://orcid.org/0000-0001-5726-2587); Email: [ongsp@eng.ucsd.edu](mailto:ongsp@eng.ucsd.edu)

### Authors

Hideyuki Komatsu – Department of NanoEngineering, University of California, San Diego, La Jolla, California 92093-0448, United States; Nissan Research Center, Nissan Motor Co., Ltd., Yokosuka, Kanagawa 237-8523, Japan; [orcid.org/0000-0002-3622-7296](https://orcid.org/0000-0002-3622-7296)

Swastika Banerjee – Department of NanoEngineering, University of California, San Diego, La Jolla, California 92093-0448, United States

Manas Likhith Holekevi Chandrappa – Department of NanoEngineering, University of California, San Diego, La Jolla, California 92093-0448, United States; [orcid.org/0000-0002-7397-3087](https://orcid.org/0000-0002-7397-3087)

Ji Qi – Materials Science and Engineering Program, University of California San Diego, La Jolla, California 92093-0448, United States

Balachandran Radhakrishnan – Alliance Innovation Laboratory, Nissan North America, Inc., Santa Clara, California 95051, United States

Shigemasa Kuwata – Alliance Innovation Laboratory, Nissan North America, Inc., Santa Clara, California 95051, United States

Kazuyuki Sakamoto – Nissan Research Center, Nissan Motor Co., Ltd., Yokosuka, Kanagawa 237-8523, Japan

Complete contact information is available at:

<https://pubs.acs.org/doi/10.1021/acs.jpcc.2c05336>

### Author Contributions

H.K. computed all calculations. All authors contributed to the discussion and interpretation of results. S.B., S.K., K.S., and S.O. supervised the work and provided valuable feedback. H.K. and S.O. wrote the main manuscript. All authors reviewed the paper.

### Notes

The authors declare no competing financial interest.

## ACKNOWLEDGMENTS

This work was primarily supported by Nissan Motor Co., Ltd., and Nissan North America, Inc. The authors also acknowledge software infrastructure (pymatgen) supported by the Materials Project, funded by the US Department of Energy, Office of Science, Office of Basic Energy Sciences, Materials Sciences and Engineering Division. The computing resources are provided by the National Energy Research Scientific Computing Center (NERSC), a U.S. Department of Energy Office of Science User Facility at Lawrence Berkeley National Laboratory and the Extreme Science and Engineering Discovery Environment (XSEDE), which is supported by National Science Foundation grant number ACI-1548562.

## REFERENCES

- Schmich, R.; Wagner, R.; Hörpel, G.; Placke, T.; Winter, M. Performance and Cost of Materials for Lithium-based Rechargeable Automotive Batteries. *Nat. Energy* **2018**, *3*, 267–278.
- Janek, J.; Zeier, W. G. A Solid Future for Battery Development. *Nat. Energy* **2016**, *1*, 16141.

- (3) Gao, Z.; Sun, H.; Fu, L.; Ye, F.; Zhang, Y.; Luo, W.; Huang, Y. Promises, Challenges, and Recent Progress of Inorganic Solid-State Electrolytes for All-Solid-State Lithium Batteries. *Adv. Mater.* **2018**, *30*, 1705702.
- (4) Xia, Y.; Zheng, J.; Wang, C.; Gu, M. Designing Principle for Ni-Rich Cathode Materials with High Energy Density for Practical Applications. *Nano Energy* **2018**, *49*, 434–452.
- (5) Julien, C. M.; Mauger, A. NCA, NCM811, and the Route to Ni-Richer Lithium-Ion Batteries. *Energies* **2020**, *13*, 6363.
- (6) Wang, X.; Ding, Y.-L.; Deng, Y.-P.; Chen, Z. Ni-Rich/Co-Poor Layered Cathode for Automotive Li-Ion Batteries: Promises and Challenges. *Adv. Energy Mater.* **2020**, *10*, 1903864.
- (7) Xu, G.-L.; Liu, X.; Daali, A.; Amine, R.; Chen, Z.; Amine, K. Challenges and Strategies to Advance High-Energy Nickel-Rich Layered Lithium Transition Metal Oxide Cathodes for Harsh Operation. *Adv. Funct. Mater.* **2020**, *30*, 2004748.
- (8) Kato, Y.; Saito, R.; Sakano, M.; Mitsui, A.; Hirayama, M.; Kanno, R. Synthesis, Structure and Lithium Ionic Conductivity of Solid Solutions of  $\text{Li}_{10}(\text{Ge}_{1-x}\text{M}_x)\text{P}_2\text{S}_{12}$  (M = Si, Sn). *J. Power Sources* **2014**, *271*, 60–64.
- (9) Kamaya, N.; Homma, K.; Yamakawa, Y.; Hirayama, M.; Kanno, R.; Yonemura, M.; Kamiyama, T.; Kato, Y.; Hama, S.; Kawamoto, K.; et al. A Lithium Superionic Conductor. *Nat. Mater.* **2011**, *10*, 682–686.
- (10) Kato, Y.; Hori, S.; Saito, T.; Suzuki, K.; Hirayama, M.; Mitsui, A.; Yonemura, M.; Iba, H.; Kanno, R. High-Power All-Solid-State Batteries using Sulfide Superionic Conductors. *Nat. Energy* **2016**, *1*, 16141.
- (11) Sun, Y.; Suzuki, K.; Hori, S.; Hirayama, M.; Kanno, R. Superionic Conductors:  $\text{Li}_{10+\delta}[\text{Sn}_y\text{Si}_{1-y}]_{1+\delta}\text{P}_{2-\delta}\text{S}_{12}$  with a  $\text{Li}_{10}\text{GeP}_2\text{S}_{12}$ -type Structure in the  $\text{Li}_3\text{PS}_4$ – $\text{Li}_4\text{SnS}_4$ – $\text{Li}_4\text{SiS}_4$  Quasi-Ternary System. *Chem. Mater.* **2017**, *29*, 5858–5864.
- (12) Kato, Y.; Hori, S.; Kanno, R.  $\text{Li}_{10}\text{GeP}_2\text{S}_{12}$ -Type Superionic Conductors: Synthesis, Structure, and Ionic Transportation. *Adv. Energy Mater.* **2020**, *10*, 2002153.
- (13) Zhu, Y.; He, X.; Mo, Y. Origin of Outstanding Stability in the Lithium Solid Electrolyte Materials: Insights from Thermodynamic Analyses Based on First-Principles Calculations. *ACS Appl. Mater. Interfaces* **2015**, *7*, 23685–23693.
- (14) Auvergniot, J.; Cassel, A.; Ledeuil, J.-B.; Viallet, V.; Seznec, V.; Dedryvère, R. Interface Stability of Argyrodite  $\text{Li}_6\text{PS}_5\text{Cl}$  Toward  $\text{LiCoO}_2$ ,  $\text{LiNi}_{1/3}\text{Co}_{1/3}\text{Mn}_{1/3}\text{O}_2$ , and  $\text{LiMn}_2\text{O}_4$  in Bulk All-Solid-State Batteries. *Chem. Mater.* **2017**, *29*, 3883–3890.
- (15) Koerver, R.; Aygün, I.; Leichtweiß, T.; Dietrich, C.; Zhang, W.; Binder, J. O.; Hartmann, P.; Zeier, W. G.; Janek, J. Capacity Fade in Solid-State Batteries: Interphase Formation and Chemomechanical Processes in Nickel-Rich Layered Oxide Cathodes and Lithium Thiophosphate Solid Electrolytes. *Chem. Mater.* **2017**, *29*, 5574–5582.
- (16) Zhang, W.; Weber, D. A.; Weigand, H.; Arlt, T.; Manke, I.; Schröder, D.; Koerver, R.; Leichtweiss, T.; Hartmann, P.; Zeier, W. G.; et al. Interfacial Processes and Influence of Composite Cathode Microstructure Controlling the Performance of All-Solid-State Lithium Batteries. *ACS Appl. Mater. Interfaces* **2017**, *9*, 17835–17845.
- (17) Xu, L.; Tang, S.; Cheng, Y.; Wang, K.; Liang, J.; Liu, C.; Cao, Y.-C.; Wei, F.; Mai, L. Interfaces in Solid-State Lithium Batteries. *Joule* **2018**, *2*, 1991–2015.
- (18) Park, K. H.; Bai, Q.; Kim, D. H.; Oh, D. Y.; Zhu, Y.; Mo, Y.; Jung, Y. S. Design Strategies, Practical Considerations, and New Solution Processes of Sulfide Solid Electrolytes for All-Solid-State Batteries. *Adv. Energy Mater.* **2018**, *8*, 1800035.
- (19) Yoshinari, T.; Koerver, R.; Hofmann, P.; Uchimoto, Y.; Zeier, W. G.; Janek, J. Interfacial Stability of Phosphate-NASICON Solid Electrolytes in Ni-Rich NCM Cathode-Based Solid-State Batteries. *ACS Appl. Mater. Interfaces* **2019**, *11*, 23244–23253.
- (20) Banerjee, A.; Tang, H.; Wang, X.; Cheng, J.-H.; Nguyen, H.; Zhang, M.; Tan, D. H.; Wynn, T. A.; Wu, E. A.; Doux, J.-M.; et al. Revealing Nanoscale Solid–Solid Interfacial Phenomena for Long-Life and High-Energy All-Solid-State Batteries. *ACS Appl. Mater. Interfaces* **2019**, *11*, 43138–43145.
- (21) Cao, D.; Zhang, Y.; Nolan, A. M.; Sun, X.; Liu, C.; Sheng, J.; Mo, Y.; Wang, Y.; Zhu, H. Stable Thiophosphate-Based All-Solid-State Lithium Batteries through Conformally Interfacial Nanocoating. *Nano Lett.* **2020**, *20*, 1483–1490.
- (22) Zhang, J.; Zheng, C.; Li, L.; Xia, Y.; Huang, H.; Gan, Y.; Liang, C.; He, X.; Tao, X.; Zhang, W. Unraveling the Intra and Intercycle Interfacial Evolution of  $\text{Li}_6\text{PS}_5\text{Cl}$ -Based All-Solid-State Lithium Batteries. *Adv. Energy Mater.* **2020**, *10*, 1903311.
- (23) Xiao, Y.; Wang, Y.; Bo, S.-H.; Kim, J. C.; Miara, L. J.; Ceder, G. Understanding Interface Stability in Solid-State Batteries. *Nat. Rev. Mater.* **2020**, *5*, 105–126.
- (24) Okuno, Y.; Haruyama, J.; Tateyama, Y. Comparative Study on Sulfide and Oxide Electrolyte Interfaces with Cathodes in All-Solid-State Battery via First-Principles Calculations. *ACS Appl. Energy Mater.* **2020**, *3*, 11061–11072.
- (25) Wang, S.; Fang, R.; Li, Y.; Liu, Y.; Xin, C.; Richter, F. H.; Nan, C.-W. Interfacial Challenges for All-Solid-State Batteries Based on Sulfide Solid Electrolytes. *J. Materiomics* **2021**, *7*, 209–218.
- (26) Sakuda, A.; Hayashi, A.; Tatsumisago, M. Interfacial Observation between  $\text{LiCoO}_2$  Electrode and  $\text{Li}_2\text{S}$ - $\text{P}_2\text{S}_5$  Solid Electrolytes of All-Solid-State Lithium Secondary Batteries using Transmission Electron Microscopy. *Chem. Mater.* **2010**, *22*, 949–956.
- (27) Ohta, N.; Takada, K.; Sakaguchi, I.; Zhang, L.; Ma, R.; Fukuda, K.; Osada, M.; Sasaki, T.  $\text{LiNbO}_3$ -Coated  $\text{LiCoO}_2$  as Cathode Material for All Solid-State Lithium Secondary Batteries. *Electrochem. Commun.* **2007**, *9*, 1486–1490.
- (28) Jalem, R.; Morishita, Y.; Okajima, T.; Takeda, H.; Kondo, Y.; Nakayama, M.; Kasuga, T. Experimental and First-Principles DFT Study on the Electrochemical Reactivity of Garnet-Type Solid Electrolytes with Carbon. *J. Mater. Chem. A* **2016**, *4*, 14371–14379.
- (29) Tan, D. H.; Wu, E. A.; Nguyen, H.; Chen, Z.; Marple, M. A.; Doux, J.-M.; Wang, X.; Yang, H.; Banerjee, A.; Meng, Y. S. Elucidating Reversible Electrochemical Redox of  $\text{Li}_6\text{PS}_5\text{Cl}$  Solid Electrolyte. *ACS Energy Lett.* **2019**, *4*, 2418–2427.
- (30) Randau, S.; Walther, F.; Neumann, A.; Schneider, Y.; Negi, R. S.; Mogwitz, B.; Sann, J.; Becker-Steinberger, K.; Danner, T.; Hein, S.; et al. On the Additive Microstructure in Composite Cathodes and Alumina-Coated Carbon Microwires for Improved All-Solid-State Batteries. *Chem. Mater.* **2021**, *33*, 1380–1393.
- (31) Jain, A.; Hautier, G.; Moore, C. J.; Ong, S. P.; Fischer, C. C.; Mueller, T.; Persson, K. A.; Ceder, G. A High-Throughput Infrastructure for Density Functional Theory Calculations. *Comput. Mater. Sci.* **2011**, *50*, 2295–2310.
- (32) Jain, A.; Ong, S. P.; Hautier, G.; Chen, W.; Richards, W. D.; Dacek, S.; Cholia, S.; Gunter, D.; Skinner, D.; Ceder, G.; et al. Commentary: The Materials Project: A Materials Genome Approach to Accelerating Materials Innovation. *APL Mater.* **2013**, *1*, 011002.
- (33) Ong, S. P.; Cholia, S.; Jain, A.; Brafman, M.; Gunter, D.; Ceder, G.; Persson, K. A. The Materials Application Programming Interface (API): A Simple, Flexible and Efficient API for Materials Data Based on REpresentational State Transfer (REST) Principles. *Comput. Mater. Sci.* **2015**, *97*, 209–215.
- (34) Kresse, G.; Furthmüller, J. Efficient Iterative Schemes for Ab Initio Total-Energy Calculations using a Plane-Wave Basis Set. *Phys. Rev. B* **1996**, *54*, 11169.
- (35) Blöchl, P. E. Projector Augmented-Wave Method. *Phys. Rev. B* **1994**, *50*, 17953.
- (36) Perdew, J. P.; Burke, K.; Ernzerhof, M. Generalized Gradient Approximation Made Simple. *Phys. Rev. Lett.* **1996**, *77*, 3865.
- (37) Boulineau, S.; Courty, M.; Tarascon, J.-M.; Viallet, V. Mechanochemical Synthesis of Li-Argyrodite  $\text{Li}_6\text{PS}_5\text{X}$  (X = Cl, Br, I) as Sulfur-Based Solid Electrolytes for All Solid State Batteries Application. *Solid State Ionics* **2012**, *221*, 1–5.
- (38) Boulineau, S.; Tarascon, J.-M.; Leriche, J.-B.; Viallet, V. Electrochemical Properties of All-Solid-State Lithium Secondary Batteries using Li-Argyrodite  $\text{Li}_6\text{PS}_5\text{Cl}$  as Solid Electrolyte. *Solid State Ionics* **2013**, *242*, 45–48.

(39) Zhu, Y.; He, X.; Mo, Y. First Principles Study on Electrochemical and Chemical Stability of Solid Electrolyte–Electrode Interfaces in All-Solid-State Li-Ion Batteries. *J. Mater. Chem. A* **2016**, *4*, 3253–3266.

(40) Richards, W. D.; Miara, L. J.; Wang, Y.; Kim, J. C.; Ceder, G. Interface Stability in Solid-State Batteries. *Chem. Mater.* **2016**, *28*, 266–273.

(41) Miara, L. J.; Richards, W. D.; Wang, Y. E.; Ceder, G. First-Principles Studies on Cation Dopants and Electrolyte Cathode Interphases for Lithium Garnets. *Chem. Mater.* **2015**, *27*, 4040–4047.

(42) Chu, I.-H.; Nguyen, H.; Hy, S.; Lin, Y.-C.; Wang, Z.; Xu, Z.; Deng, Z.; Meng, Y. S.; Ong, S. P. Insights into the Performance Limits of the  $\text{Li}_7\text{P}_3\text{S}_{11}$  Superionic Conductor: A Combined First-Principles and Experimental Study. *ACS Appl. Mater. Interfaces* **2016**, *8*, 7843–7853.

(43) Tang, H.; Deng, Z.; Lin, Z.; Wang, Z.; Chu, I.-H.; Chen, C.; Zhu, Z.; Zheng, C.; Ong, S. P. Probing Solid–Solid Interfacial Reactions in All-Solid-State Sodium-Ion Batteries with First-Principles Calculations. *Chem. Mater.* **2018**, *30*, 163–173.

(44) Deng, Z.; Zhu, Z.; Chu, I.-H.; Ong, S. P. Data-Driven First-Principles Methods for the Study and Design of Alkali Superionic Conductors. *Chem. Mater.* **2017**, *29*, 281–288.

(45) Jain, A.; Hautier, G.; Ong, S. P.; Moore, C. J.; Fischer, C. C.; Persson, K. A.; Ceder, G. Formation Enthalpies by Mixing GGA and GGA +  $U$  Calculations. *Phys. Rev. B* **2011**, *84*, 045115.

(46) The Materials Project, *Materials Data on  $\text{MnS}_2$*  by Materials Project. <https://www.osti.gov/biblio/1319031> (accessed 2022-09-14).

(47) The Materials Project, *Materials Data on  $\text{Li}(\text{MnS}_2)_2$*  by Materials Project. <https://www.osti.gov/biblio/1319939> (accessed 2022-09-14).

(48) Ozawa, K. Lithium-Ion Rechargeable Batteries with  $\text{LiCoO}_2$  and Carbon Electrodes: The  $\text{LiCoO}_2/\text{C}$  System. *Solid State Ionics* **1994**, *69*, 212–221.

(49) Sim, S.-J.; Lee, S.-H.; Jin, B.-S.; Kim, H.-S. Use of Carbon Coating on  $\text{LiNi}_{0.8}\text{Co}_{0.1}\text{Mn}_{0.1}\text{O}_2$  Cathode Material for Enhanced Performances of Lithium-Ion Batteries. *Sci. Rep.* **2020**, *10*, 11114.

(50) Xu, K. Nonaqueous Liquid Electrolytes for Lithium-Based Rechargeable Batteries. *Chem. Rev.* **2004**, *104*, 4303–4418.

(51) Xu, K. Electrolytes and Interphases in Li-Ion Batteries and Beyond. *Chem. Rev.* **2014**, *114*, 11503–11618.

(52) Min, K.; Seo, S.-W.; Song, Y. Y.; Lee, H. S.; Cho, E. A First-Principles Study of the Preventive Effects of Al and Mg Doping on the Degradation in  $\text{LiNi}_{0.8}\text{Co}_{0.1}\text{Mn}_{0.1}\text{O}_2$  Cathode Materials. *Phys. Chem. Chem. Phys.* **2017**, *19*, 1762–1769.

(53) Min, K.; Kim, K.; Jung, C.; Seo, S.-W.; Song, Y. Y.; Lee, H. S.; Shin, J.; Cho, E. A Comparative Study of Structural Changes in Lithium Nickel Cobalt Manganese Oxide as a Function of Ni Content during Delithiation Process. *J. Power Sources* **2016**, *315*, 111–119.

(54) Zhang, F.; Lou, S.; Li, S.; Yu, Z.; Liu, Q.; Dai, A.; Cao, C.; Toney, M. F.; Ge, M.; Xiao, X.; et al. Surface Regulation Enables High Stability of Single-Crystal Lithium-Ion Cathodes at High Voltage. *Nat. Commun.* **2020**, *11*, 3050.

(55) Tian, Y.; Shi, T.; Richards, W. D.; Li, J.; Kim, J. C.; Bo, S.-H.; Ceder, G. Compatibility Issues between Electrodes and Electrolytes in Solid-State Batteries. *Energy Environ. Sci.* **2017**, *10*, 1150–1166.

(56) Koerver, R.; Zhang, W.; de Biasi, L.; Schweidler, S.; Kondrakov, A. O.; Kolling, S.; Brezesinski, T.; Hartmann, P.; Zeier, W. G.; Janek, J. Chemo-Mechanical Expansion of Lithium Electrode Materials – On the Route to Mechanically Optimized All-Solid-State Batteries. *Energy Environ. Sci.* **2018**, *11*, 2142–2158.

(57) Ko, S.; Lee, S. C.; Lee, C. W.; Im, J. S. A Co-free layered  $\text{LiNi}_{0.7}\text{Mn}_{0.3}\text{O}_2$  Cathode Material for High-Energy and Long-Life Lithium-Ion Batteries. *J. Alloys Compd.* **2014**, *613*, 96–101.